1972

NUMERICAL AND WIND TUNNEL SIMULATION[Δ] OF AIRFLOW OVER AN OBSTACLE

By

Tetsuji Yamada**
Robert N. Meroney*

January 18, 1972

Submitted to

Journal of Applied Meteorology

(also presented at the National Conference
on Atmospheric Waves, American Meteorological Society,
at Salt Lake City, October 12-15, 1971)

[Δ] Research Support Under THEMIS, Office of Naval Research,
Contract No. N00014-68-A-0493-0001, Project No. NR062-414/6-6-68
(Code 458) is gratefully acknowledged.

* Associate Professor, Fluid Mechanics Program,
Colorado State University, Fort Collins.

** Postdoctoral Fellow, Colorado State University,
Fort Collins.

CEP70-71TY-RNM94

Abstract

Two dimensional airflow over a square obstacle in a stratified atmosphere is studied both numerically and experimentally as a part of a program to examine the response of stratified shear layers to non-homogeneous surface features. A wind tunnel was designed and constructed which provides the necessary very small velocities and strong stratification to simulate atmospheric lee waves. Numerical experiments show that an upstream difference scheme is not suitable to simulate strong lee wave phenomena windward of an obstacle. Its failing appears to be its large numerically generated pseudo viscosity. An improved second-order finite-difference approximation produced gravity wave motions. The numerical scheme appears to be singularity free, does not produce unwarranted interior perturbations, and realistically models streamwise boundary behavior. The details of the improved analysis were confirmed by measurements in the thermal wind tunnel.

1. Introduction

The subject of a fluid motion over obstacles has been of continuing interest to fluid dynamicists and meteorologists because it relates to such important phenomena as separation, wakes (rotors), hydraulic jumps, and mountain lee-waves.

At least four recent reviews are available for airflows over mountainous terrains (Corby, 1954; W.M.O., 1960; Krishnamurti, 1964; Lin and Cermak, 1969). Early analytical models for airflow over mountains were all based on a linear perturbation method. Queney, Lyra, Scorer and others made important contributions to develop the linear theory. Long suggested a class of stratified flows for which the nonlinear

equations could be exactly transformed into a solvable set of linear equations in 1953. Primary contributions to Long's model are found, in addition to Long's own works (Long, 1953, 1955), in Yih (1960, 1965), Drazin and Moore (1967), Miles (1968a, 1968b), Davis (1969), and Pao (1969).

Common characteristics of both linearized and nonlinear models are the assumption of two dimensionality and stationarity. The latter assumption introduces the possibility of non-unique solutions. In order to assure uniqueness, Rayleigh introduced Rayleigh friction terms in his system of equations. An alternative way to establish uniqueness is to treat the problem as an initial value problem rather than a stationary one (Krishnamurti, 1964, p. 594). However, if the problem is treated as an initial value problem, then the convenient transformation of variables which transforms the original nonlinear equation to a linear one is no longer possible (Yih, 1965). This limitation explains why research programs since the 1950's are primarily based on numerical integrations utilizing a digital computer.

Foldvik and Wurtele (1967) constructed a numerical model of an airflow over a rectangular shape mountain. They used the Boussinesq approximation to derive the vorticity equation, but friction terms were not included. Their solution developed computational instabilities from the lateral boundaries and from the obstacle; however, the instability magnitudes were small so that the majority of the field was apparently not affected. Lin and Apelt (1970) conducted numerical experiments of fluid motion over a thin barrier. Two cases were computed -- one for Re = 397, Pr = 10 and Ri = 1.58, and another for Re = 5000, Pr = 1, and Ri = 1.58, where Re, Pr, and Ri indicate Reynolds, Prandtl, and

Richardson numbers, respectively. The two results did not display considerable differences primarily because the amplitude of the lee waves generated were so small. Strong damping or diffusing effects were evident due to the finite difference scheme they used. Their upstream difference scheme has a very large pseudo (computational) viscosity which can eliminate otherwise wavy motion behind an obstacle.

This study reports a systematic investigation combining the best features of laboratory simulation and numerical modeling of the lee-wave motions arising from flows of stratified fluids over an obstacle. All nonlinear and dissipative effects are retained, and deviations from Long's model and linear theories are discussed.

2. Laboratory Simulation

The accuracy of a numerical experiment, depends on many factors, such as the particular differencing scheme used, the magnitude of grid and time increments, the boundary conditions imposed, the size of the computational area, etc. Therefore, it is necessary to investigate the reliability of numerical results by other means. If the problem is simple enough, a comparison with a known analytical solution might be possible. This is not normally the case, however, for such nonlinear problems as are described here. A laboratory experiment is extremely useful in determining the reliability of numerical results. Very few experimental results are available on stratified flow over an obstacle. Long (1955) and Davis (1969) obtained results in a water channel. Lin and Binder's (1967) experiments are the only ones available from wind tunnel experiments, although their flow characteristics were strongly limited ($0.02<Fr<0.03$, where Fr is the Froude number based on the wind

tunnel height). Model experiments in wind tunnel are very difficult, (Scorer, 1953; Cermak et.al., 1966), since similarity law requires a very strong temperature gradient and a very small velocity. Fortunately it is not impossible to have a vertical temperature gradient of $1^{o}c/cm$ and horizontal velocity of 10 cm/sec in the present wind tunnel facility. The experimental results discussed herein were specifically generated to verify any numerical scheme proposed.

Once confidence is established in numerical procedures through laboratory simulation, ~~the~~ the direct application of the numerical program to the atmosphere is reasonable. In a numerical approach it is subsequently possible to extend or change meteorological variables easily.

In this study Davis' measurements (1969) in a water channel were used to provide physical guidance in numerical analogue construction, after which the method was compared independently with wind tunnel lee-wave data produced by the authors.

Dimensions of the test section of the proposed wind tunnel are 50 cm height x 60 cm width x 450 cm length. Temperature stratification is provided by electric heaters at entrance section and along the ceiling, and by cooling panels along the wind tunnel floor. Velocities were measured utilizing a smoke-wire technique developed at the Fluid Dynamics and Diffusion Laboratory, Colorado State University. Thermocouples were used for the temperature measurements (See Yamada and Meroney (1971) for the detailed description of the wind tunnel facility and instrumentation).

3. Formulation of Problem

The formulation of the problem is initially based on the assumptions of two-dimensionality and incompressibility of the fluid. X and z

coordinates are to be taken in the direction perpendicular to the obstacle and vertical, respectively. Then the equation of continuity is written as

$$\frac{\partial u}{\partial x} + \frac{\partial w}{\partial z} = 0 \quad , \tag{1}$$

where u and w are velocity components in x and z direction, respectively. Vorticity transport equation is as follows

$$\frac{D\zeta}{Dt} = K\nabla^2\zeta + \frac{g}{T}\frac{\partial T}{\partial x} \quad , \tag{2}$$

where ζ is a vorticity component in the y direction (which is parallel to the obstacle)

$$\zeta = \frac{\partial w}{\partial x} - \frac{\partial u}{\partial z} \quad . \tag{3}$$

T is absolute temperature, and K is a total eddy viscosity.

$\frac{D}{Dt}$ is the Eulerian operator which is expressed as

$$\frac{D}{Dt} = \frac{\partial}{\partial t} + u\frac{\partial}{\partial x} + w\frac{\partial}{\partial z} \quad .$$

∇^2 is the Laplacian operator in two dimensional space $\nabla^2 = \frac{\partial^2}{\partial x^2} + \frac{\partial^2}{\partial z^2}$.

The continuity equation of incompressible fluid (1) permits the existence of a stream function ψ such that

$$u = -\frac{\partial \psi}{\partial z} \quad \text{and} \quad w = \frac{\partial \psi}{\partial x} \quad . \tag{4}$$

Introduction of a stream function ψ guarantees that the continuity equation (1) is always satisfied. Substituting the stream function into Eq. (3) we obtain a relation between the vorticity ζ and the stream function ψ as

$$\nabla^2\psi = \zeta \tag{5}$$

The equation of energy in this case is given as

$$\frac{DT}{Dt} = K'\nabla^2 T \tag{6}$$

where K' is a total heat diffusivity.

The set of equations (2), (5) and (6) with the definition of the stream function (4) are to be integrated numerically with appropriate boundary and initial conditions.

4. Numerical Procedure

The primary difficulty associated with the approximation of a partial differential equation by a finite difference equation is due to the existence of nonlinear inertial terms such as $u\frac{\partial \zeta}{\partial x}$ or $w\frac{\partial \zeta}{\partial z}$. If one uses a forward difference for a time derivative and a centered difference for a space derivative then the difference equation for a differential equation $\partial\zeta/\partial t + u\,\partial\zeta/\partial x = 0$ is unconditionally unstable (Richtmyer and Morton, 1967, p. 292). Hence, no matter how small a time step is chosen, small errors introduced in the computation grow without limit.

A solution to this instability has been provided by a "forward-backward" molecule which replaces convection terms, for example $u\frac{\partial \zeta}{\partial x}$, by

$$\left(u\frac{\partial \zeta}{\partial x}\right)^n_{j,\ell} = u^n_{j,\ell}\,\frac{\zeta^n_{j,\ell} - \zeta^n_{j-1,\ell}}{\delta x} \quad \text{when} \quad u^n_{j,\ell} \geq 0\,,$$

$$= u^n_{j,\ell}\,\frac{\zeta^n_{j+1,\ell} - \zeta^n_{j,\ell}}{\delta x} \quad \text{when} \quad u^n_{j,\ell} < 0\,,$$

where δx is the space increment in x direction. This relation states that when the velocity $u^n_{j,\ell}$ is positive then the space derivative

is approximated by a backward difference, and when $u^n_{j,\ell}$ is negative a forward difference is used. In this way the direction of the convection is always the same as that of the local velocity components. All variables are transported from the upstream side of the point in a local sense, where subscript j and ℓ are j^{th} and ℓ^{th} grid points in x and z direction, respectively. In the same manner, the superscript n stands for the n^{th} time step of integration. $n = 1$ is an initial time. The final form of a finite difference approximation of the vorticity transport equation (2) is obtained by replacing the diffusion terms by centered differences while the nonlinear terms are approximated by the upstream numerical system.

The magnitude of the stream function is obtained by solving the Poisson equation with known vorticity values. Herein a successive over-relaxation (S.O.R.) method was utilized. The convergence criterion of the iteration procedure was:

$$|\psi^{r+1} - \psi^{r}|_{\max} < \delta$$

i.e., if the absolute value of the maximum difference between the $(r+1)$st iteration and the previous r th iteration is less than δ then the iteration is stopped. δ should be determined by numerical experiments and here we adjusted δ from 0.01 to 0.10 depending on the magnitude of the stream function at the top boundary. The finite difference expression for the energy equation has a very similar appearance to that of the vorticity transport equation.

The condition which should be satisfied in order to maintain stability in the finite difference expression of the vorticity equation (2) is

$$\delta t \leq \frac{C}{\frac{|u|_{\max}}{\delta x} + \frac{|w|_{\max}}{\delta z} + \frac{2k}{\delta x^2} + \frac{2k}{\delta z^2}}, \qquad (7)$$

where δt is a time increment in the finite-difference equation, and the constant value C is $0<C<1$, and $|u|_{max}$ and $|w|_{max}$ are the magnitudes of the maximum velocity components u and w, respectively, in the entire computation region. The stability criterion is thus a variable depending upon the magnitude of each set of newly calculated velocity components. In practice $|u|_{max}$ and $|w|_{max}$ were calculated at each time step and δt was selected such that it satisfied the stability condition (7).

It is desirable to choose δt as large as possible within the computational stability criterion in order to save computation time. If a larger time step is chosen, however, more iterations may be required in the solution of the Poisson equation because the source terms (vorticities) vary by larger steps also. Since the associated iteration technique is a time consuming calculation, a larger time increment does not necessarily save computational time as one might expect.

It is necessary to specify both boundary and initial conditions to obtain a set of unique solutions. Boundary conditions for the vorticity transport equation cannot be given directly. However, they are closely related to interior values of vorticity and stream functions by means of a Taylor's series expansion. For rigid boundaries this relation is very simple and may be derived analytically from the known boundary conditions of velocities and stream functions.

In this study both the upper and the lower boundaries are rigid and a no-slip velocity condition is used. i.e.,

$$u = w = 0 \quad \text{at} \quad z = 0 \quad \text{and} \quad z = H$$

where H is the height of the top boundary. The stream function is assigned a zero value along the bottom boundary and a constant value is maintained along the top boundary. The final expression for the boundary values of vorticities along rigid boundaries is:

$$\zeta_{\text{bound}} = \frac{3}{(\delta z)^2} \left(\psi_{\text{int}} - \psi_{\text{bound}}\right) - \frac{1}{2} \zeta_{\text{int}} ,$$

where ζ_{bound} and ψ_{bound} are the boundary values of vorticity and stream function, respectively. Subscript "int" indicates the values at one grid inside from the boundary.

Boundary conditions at the up-and down-stream boundaries are more difficult and must be determined more or less empirically. Lateral boundary conditions were sought which imposed the least severe restrictions on the solutions in the interior region, i.e., such that no distorted values at the boundaries propagate into the interior area. The following boundary conditions have been determined from numerical experiments to give the least apparent restrictions and the least distortions. Linear extrapolation formulae were used for all dependent variables ψ, ζ, and T. For example the upstream boundary values of stream functions, $\psi_{1,\ell,}$ are computed from

$$\psi_{1,\ell} = 2\psi_{2,\ell} - \psi_{3,\ell} ,$$

where $\psi_{2,\ell}$ and $\psi_{3,\ell}$ are the values one and two grid interior the region, respectively. The physical implication of the above condition as follows: Streamlines are assumed to change linearly i.e., maintain constant slopes at the lateral boundaries. Thus,

$$\frac{\partial^2 \psi}{\partial x^2} = \frac{\partial^3 \psi}{\partial x^3} = \frac{\partial^4 \psi}{\partial x^4} = \ldots\ldots = 0 .$$

In terms of velocity component w this requires $\frac{\partial w}{\partial x} = 0$. However, since this numerical model is formulated in terms of the vorticity equation one needs boundary conditions for vorticities at the lateral boundaries. With the assumption that the stream function varies linearly at the lateral system boundaries one may conclude from

$$\frac{\partial^2 \zeta}{\partial x^2} = \frac{\partial^4 \psi}{\partial x^4} + \frac{\partial^2}{\partial z^2}\left(\frac{\partial^2 \psi}{\partial x^2}\right)$$

that

$$\frac{\partial^2 \zeta}{\partial x^2} = 0 \quad .$$

Boundary conditions for the energy equation at both streamwise boundaries are similarly

$$\frac{\partial^2 T}{\partial x^2} = 0 \quad .$$

To integrate the set of the equations described above, initial values must be specified to initialize the numerical integration. Hence, initial velocity components u and w are originally given, to obey continuity and the vorticities and stream functions are initialized by their respective definitions.

Numerical integrations and laboratory experiments have been conducted in such a manner that they may be directly compared. Therefore, it was convenient to use the same coordinate system in each case. Wind tunnel test section is 50 cm height x 60 cm width x 450 cm length. Hence, a region of comparable size was utilized in the numerical computation (see Fig. 1). The area was divided by a 81 x 16 square mesh whose dimension is 4 x 4 cm. Therefore, a 60 cm height x 320 cm length area is the computational region - about the same size as the effective wind tunnel test section area.

5. Test Computation of Airflow over an Obstacle

The first computation of airflow over an obstacle was conducted under the same conditions for which the best lee waves are observed in Davis' paper (1969). In his paper, the characteristic parameter is expressed by k which is the inverse of the Froude number based on the characteristic length H/π, where H is the channel height. Since $k = 1.5$ gave the strongest lee wave result, we used this value in the computation, which is equivalent to $Fr = 0.2122$ in our terminology.

In his paper, dynamic pressure and vertical density gradient at the far upstream boundary are kept constant (Long's model). From these conditions, an upstream temperature distribution was calculated. The resulting temperature varies almost linearly except for the region very close to the surface. This temperature distribution was used as an initial value. Numerical integration was carried out in 150 steps and results were plotted. Figure 2 shows very weak first wave crests somewhere near $x = 80$ cm but compared to Davis' result, (included in the same figure), they are very small.

If a comparison, however, is made with a result obtained in a neutral atmosphere (no stratification) which is also included in Fig. 2, we can see definite effects of stratification. In the stratified case, streamlines over the obstacle have been displaced downward because of the negative buoyancy forces introduced by the density difference between a particle and its surroundings. This force together with the requirement of continuity bends streamlines downward behind the obstacle. Because of its inertia, a particle drops down beyond its equilibrium position and encounters a positive buoyancy

force which again would lift the particle beyond its equilibrium if no dissipation of energy exists. The initial calculations obtained displayed some interestesting aspects of stratified airflow over an obstacle. However, they did not generate lee waves downwind of the obstacle.

Several authors have suggested that the upstream finite-difference approximation introduces a strong damping effect: which may under certain circumstances modify or control the solution.
Let us examine how a computational viscosity is introduced. The one dimensional, unsteady, and incompressible vorticity transport equation without a diffusion term is expressed as

$$\frac{\partial \zeta}{\partial t} + u \frac{\partial \zeta}{\partial x} = 0 \quad .$$

Its first order approximation in the upstream scheme is given as

$$\frac{\zeta_j^{n+1} - \zeta_j^n}{\delta t} + u \frac{\zeta_j^n - \zeta_{j-1}^n}{\delta x} = 0 \quad , \tag{8}$$

when u is not negative and a forward approximation is used for the time derivative. Substituting the Taylor's series expansions for ζ_{j-1}^n and ζ_j^{n+1} about ζ_j^n (neglecting higher order terms than δx^3 or δt^3) into the above expression we obtain

$$\frac{\zeta_j^{n+1} - \zeta_j^n}{\delta t} + u \frac{\zeta_j^n - \zeta_{j-1}^n}{\delta x}$$

$$= \frac{\partial \zeta}{\partial t} + u \frac{\partial \zeta}{\partial x} - \frac{u \delta x}{2} \left(1 - \frac{u \delta t}{\delta x}\right) \frac{\partial^2 \zeta}{\partial t^2} + \ldots \tag{9}$$

where the relation

$$\frac{\partial^2 \zeta}{\partial t^2} = u^2 \frac{\partial^2 \zeta}{\partial x^2}$$

is used from the original equation assuming u is constant. A similar expression is obtained when u is negative. If the finite difference equation (8) is solved exactly then the differential equation becomes (from Eq.9),

$$\frac{\partial \zeta}{\partial t} + u \frac{\partial \zeta}{\partial x} = \frac{|u| \delta x}{2} \left(1 - \frac{|u| \delta t}{\delta x}\right) \frac{\partial^2 \zeta}{\partial x^2} \quad .$$

where the absolute value of u is used so that this expression is valid for both positive and non-positive u. The term

$$\nu_p = \frac{|u| \delta x}{2} \left(1 - \frac{|u| \delta t}{\delta x}\right)$$

has been called the pseudo viscosity or pseudo diffusivity (Molenkamp, 1968). Molenkamp evaluated ν_p for typical thermal convection situations in the atmosphere and numerical values were of the order of $35 m^2 sec^{-1}$, which is comparable with typical measured turbulent viscosities ranging from 0 to 40 $m^2 sec^{-1}$. In the previous calculation (Fig. 2), $\delta t = 0.05729$ sec and $\delta x = 4$ cm when $t = 8.96$ sec. Therefore, pseudo viscosity ν_p has a maximum value

$$(\nu_p)_{max} = \frac{\delta x^2}{8 \delta t} = \frac{4^2}{0.05729} = 34.91 \text{ cm}^2/\text{sec}$$

when $u = 34.91$ cm/sec.

Since the pseudo viscosity appears to be as large as 150 times the actual viscosity, ($\nu_p = 29$ cm^2/sec when $u = 20$ cm/sec), it is inappropriate to simulate wind tunnel experiments by the upstream difference approximation. (For detailed discussions about the concept of pseudo viscosity see Crowley 1967, 1968; Molenkamp, 1968; and Orville, 1968).

One is now led to search for some second order method with a smaller damping effect. Arakawa's (1966) explicit scheme is one of such differencing techniques. Molenkamp (1968) showed that Arakawa's scheme has increased accuracy compared with the upstream difference method just discussed.

Arakawa's scheme replaces the inertial terms in the vorticity equation by centered differences to obtain computational stability incorporating the nonlinear terms. Arakawa (1966) developed his finite difference scheme for the vorticity transport equation in such a manner that it conserves the mean vorticity, the mean kinetic energy, and the mean square vorticity in a closed domain. Since we found the upstream difference approximation system is not appropriate to simulate wave motions behind an obstacle and Arakawa's scheme has been proven to often have better accuracy, we reprogrammed using this scheme. The time derivative is approximated by a centered difference. Both the diffusion term $K(\frac{\partial^2\zeta}{\partial x^2} + \frac{\partial^2\zeta}{\partial z^2})$ and the buoyancy term $\frac{g}{T}\frac{\partial T}{\partial x}$ are also approximated by centered difference molecules. This scheme was expected to give a better result, and it is computationally stable if an appropriate integration time step is used.

6. Mixed Scheme with Upstream Difference

The first computation in Arakawa's scheme produced very short wave length (two grid intervals) disturbances in front of the obstacle. These disturbances appear to propagate backwards against the mean flow with time. The speed of propagation was roughly the same as the basic flow. Such errors are generally considered to be a result produced by a large truncation error at a sharp discontinuity of the boundary

(a step change obstacle). Foldvik and Wurtele (1967) have observed the same kind of perturbations in front of their rectangular obstacle.

To eliminate these computational modes the numerical area was divided into two regions - one in front of the obstacle and another over and behind the obstacle. The downwind region was approximated by Arakawa's scheme and the upstream difference system was used in the upwind one. It was expected that the upstream scheme could disperse numerical errors (waves with two grid length) introduced in front of the obstacle by its large numerical damping.

Fortunately, available laboratory and field observations suggest that physical waves which actually propagate upstream from an obstacle have long wave characteristics which are much less affected by the numerical damping effect in upstream difference approximation. Thus it is expected that all physical waves are retained under this scheme while short wave computational modes upstream of the obstacle will be damped out quickly.

Another procedure to stabilize the field to numerically generated instabilities was suggested by the test computation. The numerical integration must be conducted for a comparatively long time to reach steady state. There appeared irregular variations with time, however, which do not actually represent any physical phenomenon. Hence it was decided to insert, every ten to twenty integration time steps, an upstream representation for the inertia terms to stabilize the field. This is a better method than a smoothing done in arbitrary nanners (such as to take arithmatic means) since here smoothing retains general character of Navier-Stokes equation.

The result of a test calculation gives pictures which do not show any computationally introduced errors. Contour lines of stream functions at different integration times are shown in Fig. 3. Here we can clearly perceive the development of lee waves behind the obstacle with time. Two waves are observed at t = 20.84 sec. The amplitude of the first wave is about the same magnitude as the obstacle height. However the wave length measured from the picture is about 76 cm which is much shorter than 100 cm as predicted by

$$\lambda = \frac{2\pi H}{\sqrt{F_r^{-2} - \pi^2}}$$

where λ is a wave length, and H is a characteristic length taken as a wind tunnel height.

The wave patterns obtained by the present analysis agree with Long's experimental results (Fig. 8, pp. 351, Long, 1955) where Fr = 0.20 and the ratio of obstacle height to that of water channel $\beta = 0.2$; while in the present computation Fr = 0.21 and $\beta = 0.13$. Although Davis' result in Fig. 2-6 appears to have stronger amplitude lee waves it should be noted that the figure has about twice as large a vertical scale as the rest of figures; height of his water channel was 36 cm while that of present computational region was [illegible] cm. Moreover, dimensionless fence height, β, was 0.2 which is approximately double the obstacle height in Fig. 3. The linearized theory predicts that the location of the first wave crests is 3/4 wave length downwind from the top of the obstacle. In most all laboratory experiments, however, it has appeared that the first wave crests were very much further displaced downstream (Long, 1955; Lin and Binder, 1967; Davis, 1969).

Furthermore, wave lengths were observed to increase with height. Thus there existed a wave phase shift in the vertical direction. Wind tunnel experiments by Lin and Binder (1967, Fig. 40) noted a functional variation of wave length with height and Froude number. The present numerical model contains both features, increased wave length and phase shift with height.

Horizontal velocity profiles at various locations at t = 20.84 sec. are included in Fig. 3-d. Initially (t = 0) they were uniformly distributed. Very high velocities are obtained over and downstream of the obstacle which are commonly observed in the field and laboratory. It is noticed that the velocity profile at the upstream boundary is modified from the original uniform distribution by the disturbances propagating upstream from the obstacle. It means that upstream difference scheme utilized in the front region of the obstacle did not eliminate long waves traveling upstream from the obstacle, but completely filtered out short waves associated with computational modes. Therefore, the present numerical model allows modifications of velocity and temperature profiles at an upstream boundary, which are caused by the disturbances travelling upstream generated by the obstacle. All existing analytical treatments requires pre-specification of the variable profiles at the upstream boundary and cannot include the effects of upstream travelling disturbances. Long's model requires constancy of dynamic pressure and of the vertical density gradient with height at the far upstream boundary. Consequently Long's model cannot consider any blocking effect of the obstacle since this phenomenon completely changes the upstream boundary condition. Moreover, the

present numerical model is more flexible since one can impose arbitrary upstream initial values, for example, ground inversion, elevated inversion, neutral, or lapse condition.

7. Control Comparison with Wind Tunnel Result

The present numerical scheme has shown qualitative agreement with other water channel laboratory investigations and analytical predictions. It is not, however, possible to conduct a precise quantitative comparison: towing tank experiments give free-slip conditions at the boundary but atmospheric motion include the shear effect of a velocity profile. Therefore, it is desirable to compare the numerical result with a wind tunnel model, where a more realistic shear layer is modeled. A laboratory result is first discussed, which exhibits waves behind a square obstacle (8cm x 8cm). Then a numerical simulation of the same flow is conducted for quantitative comparison.

Figure 4 displays streamlines obtained from a smoke visualization picture. A five-second exposure time indicated that the flow was very steady. The smoke was dispersed very rapidly under the first wave crest by the presence of a turbulent rotor. Such motions were reported by both prototype (W.M.O., 1960) and previous laboratory observations (Long, 1955; Lin and Binder, 1967; Davis, 1969).

Temperature contour lines (Fig. 5) have been constructed from the temperature profiles at various locations. Isotherms taken from experiments performed on different days show very close agreement, which indicates good laboratory reproducibility.

Since the measured temperature profiles were not linear with height (see Fig. 6) some difficulty arose to evaluate Froude number which is the characteristic parameter of the flow. Temperature increases fairly sharply ($\frac{\partial T}{\partial z}$ ~ 1.2° C/cm) from the surface to a certain height (~ 13cm) and subsequently decreases to the center of the wind tunnel.

There exists another sharp temperature increase as one approaches the wind tunnel ceiling where large elctric heaters are mounted. If there is no flow blowing inside the tunnel linear variation of temperature with height is expected. But basic wind blowing over the surface and ceiling increases heat transfer from the boundaries resulted in sharper temperature gradients there.

Long (1955) commented on a similar difficulty when computing the Froude number. His density profile showed nearly constant regions close to both top and bottom boundaries. Long found if an averaged value of stability was used to compute Froude number then the observed wave length closely agreed with the predicted value from the theory. Here a similar idea was used; two stabilities were computed, one for the lower layer ($0 \leq z \leq 13$cm) and another for the upper layer (13 cm < z < 40cm). Then the arithmatic mean was taken to evaluate Froude number.

A numerical experiment was performed for identical flow conditions. Contour lines of stream function, vorticity and temperature are shown in Fig. 7. General agreement with the wind tunnel experiment (Fig. 4, 5) was obtained. The wave amplitude in the numerical model was not as large.

Temperature profiles at various locations for both wind tunnel and numerical experiments are presented in Fig. 8. The location $x = 0$ corresponds to the upwind edge of the obstacle. A dashed line in the first figure indicates the initial distribution provided for the numerical integration. Initial profiles can be arbitrary; however, for a faster convergence a reasonable initialization is desirable. An averaged temperature distribution for the clean wind tunnel field was used as an initializing distribution (Fig. 6). Data at $x = -20$ cm in Fig. 8 show clear evidence of upstream flow modification by the existence of an obstacle. Numerical temperature distributions at $x = 12$, 16, and 20 cm appear to simulate regions of overturning instability $(\frac{\partial T}{\partial z} < 0)$, where the flow was supposed to be very unstable. According to Long's analysis (1955) this region should correspond to a reversed flow area.

The existence of turbulent motion under the first wave crest can be seen from the temperature profiles at $x = 48$, and 60 cm. Experimental results at these locations show constant values near the ground as a result of strong turbulent mixing. The numerical model failed to simulate the phenomena in this region primarily due to insufficient numbers of grid points near the ground where the temperature varies rapidly.

A detailed examination of the flow field immediately behind the obstacle is shown in Fig. 9. The square obstacle is indicated by a double hatched area, and the effective mountain is represented by a single hatched region. A streamline and the observed flow directions are as indicated. Velocity profiles at $x = 12$, 40, and 60 cm were

obtained from smoke wire photographs. The velocity distribution sketched at $x = 12$ cm represents an average from two pictures taken three minutes apart. Both pictures presented similar profiles; therefore, the result shown here seems to be reliable.

The motion inside the separated region (or core) was quite different from that observed for neutral density flows. Velocity close to the surface was positive, a negative flow was observed above it, and the flow reversed again outside the core (see Fig. 9). The temperature distributions at $x = 12$, 16, and 20 cm also exhibit alternative positive and negative gradients.

This peculiar motion may be explained as following: A fluid particle trapped into the core region originates at some high temperature level (Fig. 5). The particle is less dense than the surrounding strata, and thus buoyancy forces drive a counterclockwise circulation.

8. Conclusions on Numerical Simulation of Strong Gravity Effects

A simple explicit upstream finite-difference system failed to produce observed lee waves behind a finite height obstacle placed in the wind tunnel. Large pseudo-viscosity introduced by the upstream difference scheme appears to introduce a large numerical viscosity. A Mixed-Arakawa's scheme was tested and found to give reasonable results.

A sequence of possible models were examined to find suitable boundary conditions at the up and down-stream boundaries. It was found that when linear extrapolation formulae were used, physically reasonable results were obtained.

A wind tunnel facility provided a more realistic simulation of airflow over a mountain compared with a towing tank. The wind tunnel proved to be a valuable diagnostic tool to justify and analyze the present numerical model.

Research support under THEMIS, Office of Naval Research, Contract No. N00014-68-A-0493-0001, Project No. NR 062-41416-6-68 (Code 438) is gratefuly acknowledged. The authors are especially obliged to the Computer Center, Colorado State University, which provided a fund for a large portion of the numerical work.

REFERENCES

Arakawa, A., 1966; Computational Design for Long-Term Numerical Integration of the Equations of Fluid Motion: Two-Dimensional Incompressible Flow, Part 1, J. Comp. Physics, Vol. 1, No. 1, pp. 119-143.

Cermak, J. E., et al., 1966; "Simulation of Atmospheric Motion by Wind Tunnel Flows," CER66-JEC-VAS-EJP-GJB-HC-RNM-SI-17, Fluid Dynamics and Diffusion Lab., Colorado State University.

Corby, G. A., 1954; "The Airflow over Mountains," Quart. J. R. Met. Soc., 80, pp. 491-521.

Crowley, W. P., 1967; "Second-Order Numerical Advection," J. Comp. Physics, Vol. I, No. 4, pp. 471-484.

Crowley, W. P., 1968; "Numerical Advection Experiments," Monthly Weather Rev., Vol. 97, No. I, pp. 1-11.

Davis, R. E., 1969; "Two-Dimensional Flow of a Stratified Fluid Over an Obstacle," J. Fluid Mech., Vol. 36, pp. 127-143.

Drazin, P. G. and Moore, D. W., 1967; "Steady Two-Dimensional Flow of Variable Density Over an Obstacle," J. Fluid Mech., Vol. 28, pp. 353-370.

Foldvik, A. and Wurtele, M. G., 1967; "The Computation of the Transient Gravity Wave," Geophys. J. R. Astr. Soc., 13, pp. 167-185.

Krishnamurti, T. N., 1964; "Theory of Two-Dimensional Mountain Waves," Review of Geophysics, Vol. 2, No. 4, pp. 593-624.

Lin, J. T., and Binder, G. J., 1967; "Simulation of Mountain Lee-Waves in a Wind Tunnel," Fluid Dynamics and Diffusion Lab., U.S. Army Research Grant DA-AMC-28-043-65-G20, Colorado State University.

Lin, J. T. and Cermak, J. E., 1969; "Dynamics of Stably Stratified Flows," Project THEMIS, Tech. Rep. No. 4, CER69-70JTL2, Fluid Dynamics and Diffusion Laboratory, Colorado State University, Fort Collins, Colorado, 167 p.

Lin, J. T., and Apelt, C. J., 1970; "Stratified Flow over an Obstacle, A Numerical Experiment," Project THEMIS, Tech. Rep. No. 7, CER69-70JTL-CJA25, Fluid Dynamics and Diffusion Laboratory, Colorado State University, Fort Collins, Colorado, 78 p.

Long, R. R., 1953; "Some Aspects of the Flow of Stratified Fluids, I: A Theoretical Investigation," Tellus, 5, pp. 42-58.

Long, R. R., 1955; "Some Aspects of the Flow of Stratified Fluids, III: Continuous Density Gradients," Tellus, 7, pp. 241-357.

Miles, J. W., 1968a; "Lee Waves in a Stratified Flow, Pt. I, Thin Barrier," J. Fluid Mech., Vol. 32, pp. 549-567.

Miles, J. W., 1968b; "Lee Waves in a Stratified Flow, Pt. II, Semi-Circular Obstacle," J. Fluid Mech., Vol. 33, pp. 803-814.

Molenkamp, C. R., 1968; "Accuracy of Finite-Difference Methods Applied to the Advection Equation," J. Appl. Meteor., Vol. 7, pp. 160-167.

Orville, H. D., 1968; "Comments on 'Accuracy of Finite-Difference Methods Applied to the Advection Equation,'" J. Appl. Meteor., Vol. 7, No. 5, pp. 938.

Pao, Y. H., 1969; "Inviscid Flows of Stably Stratified Fluids Over Barriers," Quart. J. R. Met. Soc., Vol. 95, No. 403, pp. 104-118.

Richtmyer, R. D. and Morton, K. W., 1967; "Difference Methods for Initial-Value Problems," Interscience Publishers.

Scorer, R. S., 1953; "Theory of Airflow Over Mountains, II. The Flow Over a Ridge," Quart. J. R. Met. Soc., 79, pp. 70-83.

Yih, C. S., 1960; "Exact Solutions for Steady Two-Dimensional Flow of a Stratified Fluid," J. Fluid Mech., Vol. 9, pp. 161-174.

Yih, C. S., 1965; "Dynamics of Nonhomogeneous Fluids," MacMillan, p. 306.

W.M.O., 1960; "The Airflow over Mountains," World Meteorological Organization, Technical Note No. 34, 135 pp.

Yamada, T., and Meroney, R. N., 1971; "Numerical and Wind Tunnel Simulation of Stratified Shear Layers to Nonhomogeneous Surface Features," CER70-71TY-RNM62, Fluid Dynamics and Diffusion Laboratory, College of Engineering, Colorado State University, Fort Collins, Colorado.

LIST OF FIGURES

Fig. 9 Detailed picture of the flow behind an obstacle (Fr = 0.126). Double hatched area is the original obstacle. Hatched region in addition to the physical obstacle may represent an effective shape of obstacle.

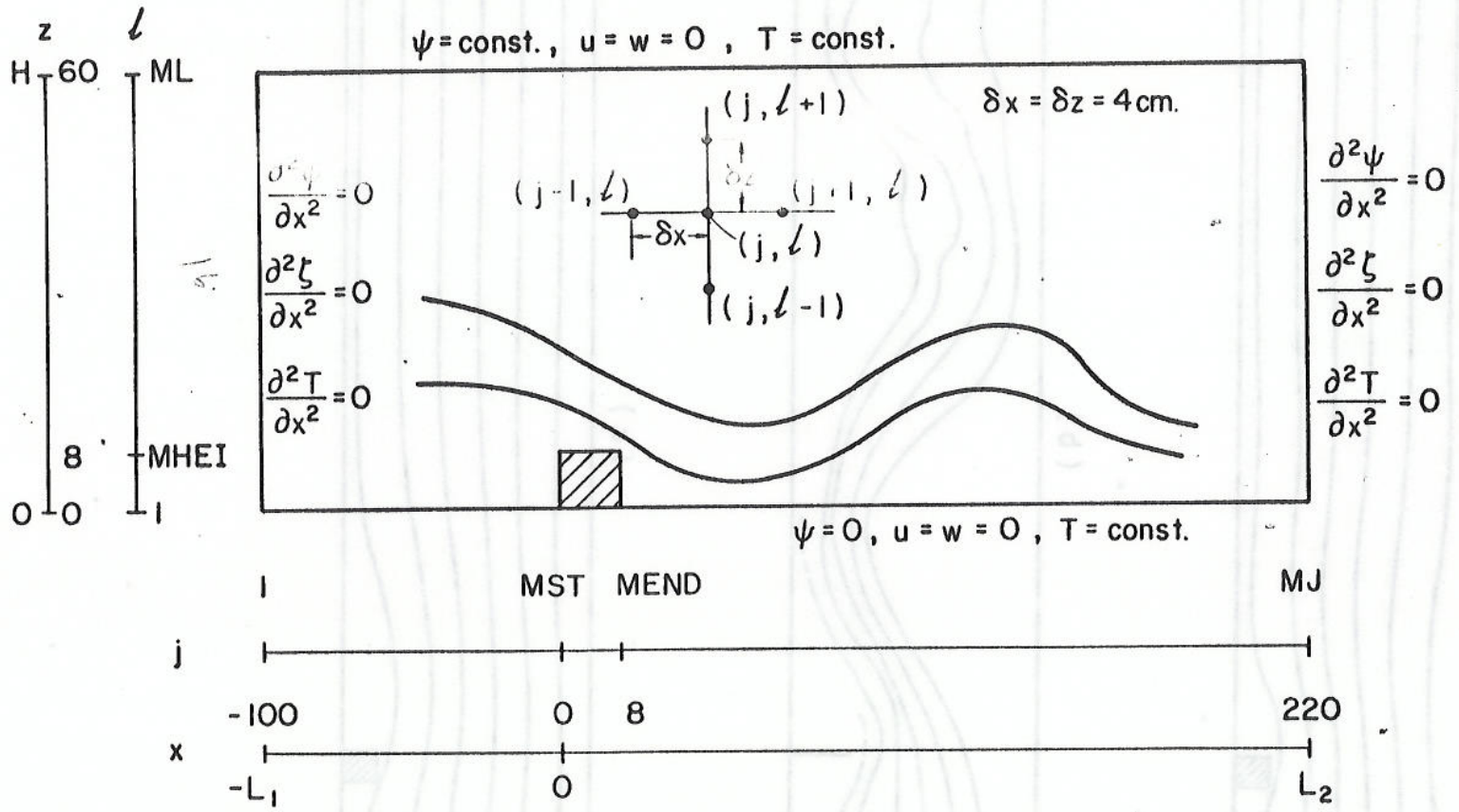
z
ℓ
H
60
ML
8
MHEI
0
0
1
ψ = const., u = w = 0, T = const.
δx = δz = 4cm.
(j, ℓ+1)
(j-1, ℓ)
(j+1, ℓ)
(j, ℓ)
(j, ℓ-1)
δx
δz
∂²ψ/∂x² = 0
∂²ζ/∂x² = 0
∂²T/∂x² = 0
ψ = 0, u = w = 0, T = const.
I
MST
MEND
MJ
j
-100
0
8
220
x
-L1
0
L2

(a)

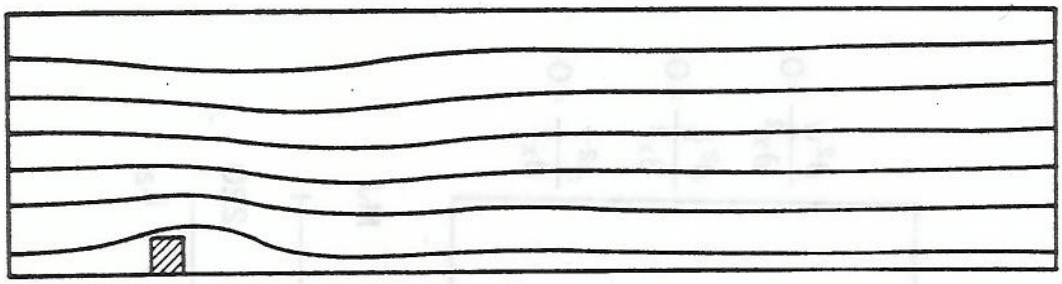

(b)

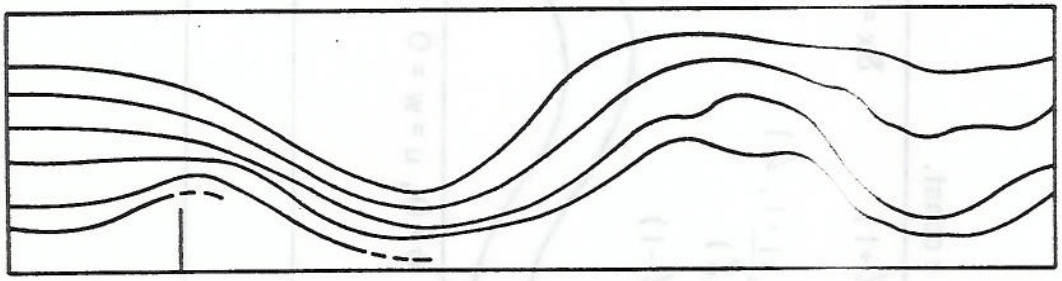

(c)

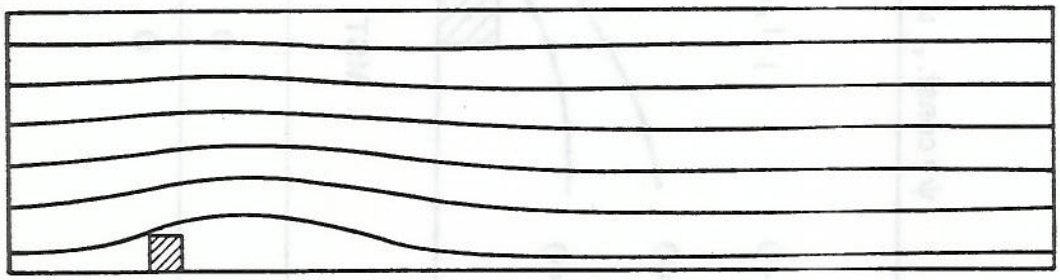

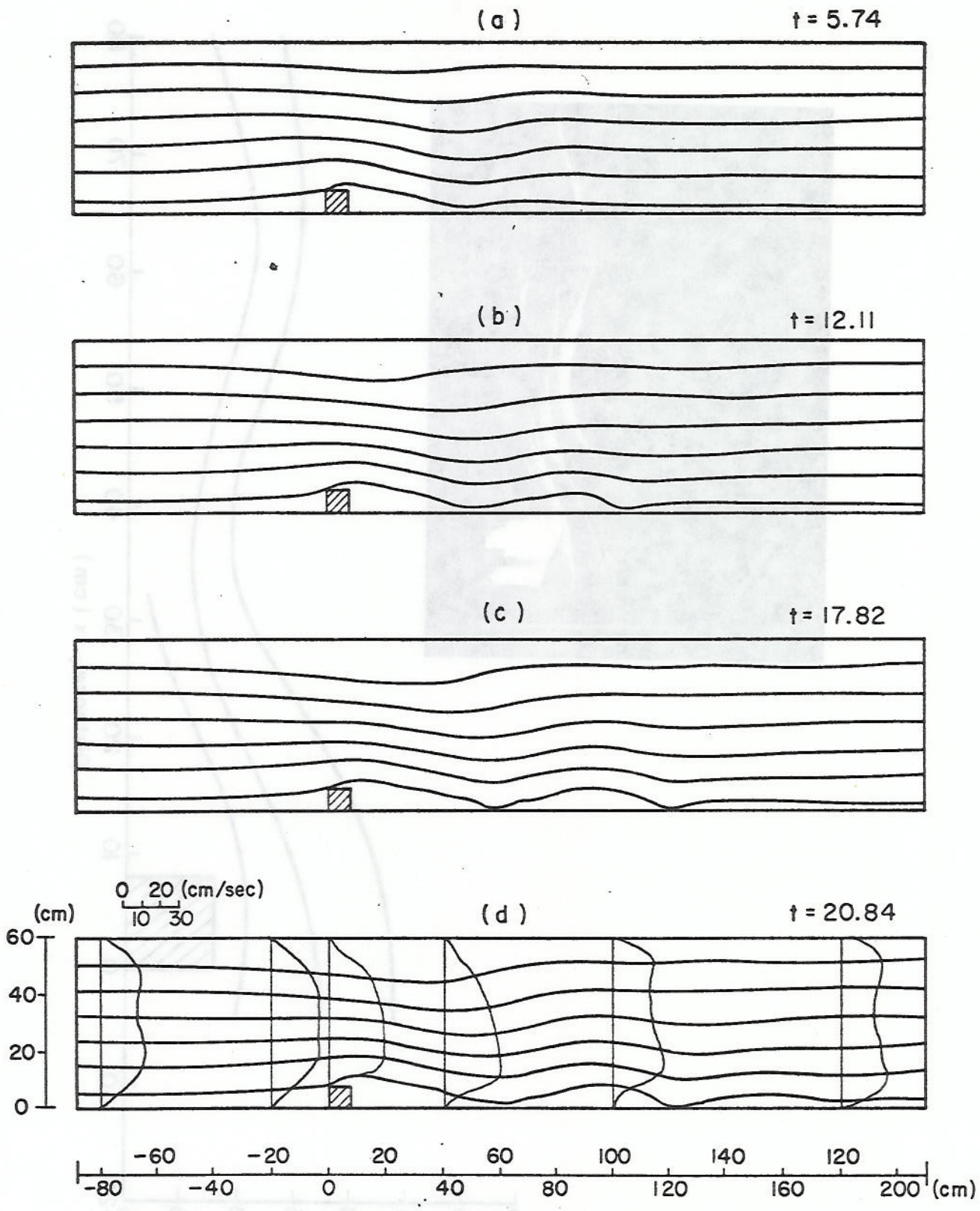
(a)
t = 5.74
(b)
t = 12.11
(c)
t = 17.82
0 20 (cm/sec)
10 30
(cm)
(d)
t = 20.84
60
40
20
0
-60
-20
20
60
100
140
120
-80
-40
0
40
80
120
160
200
(cm)

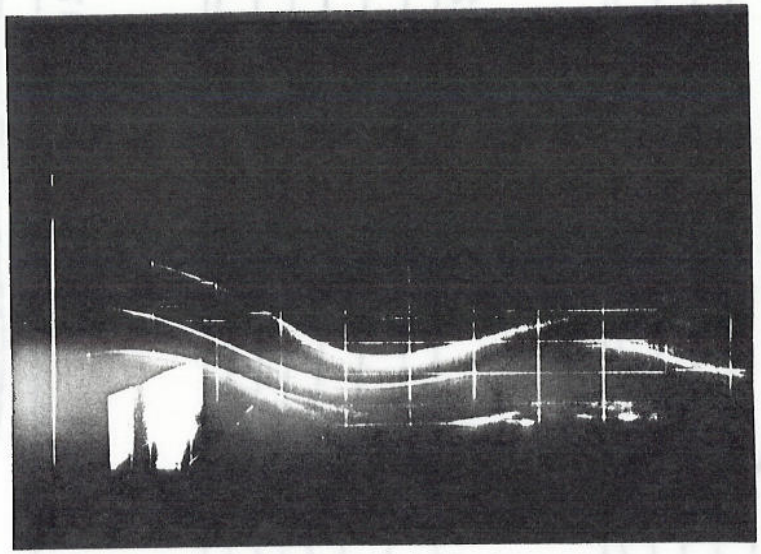

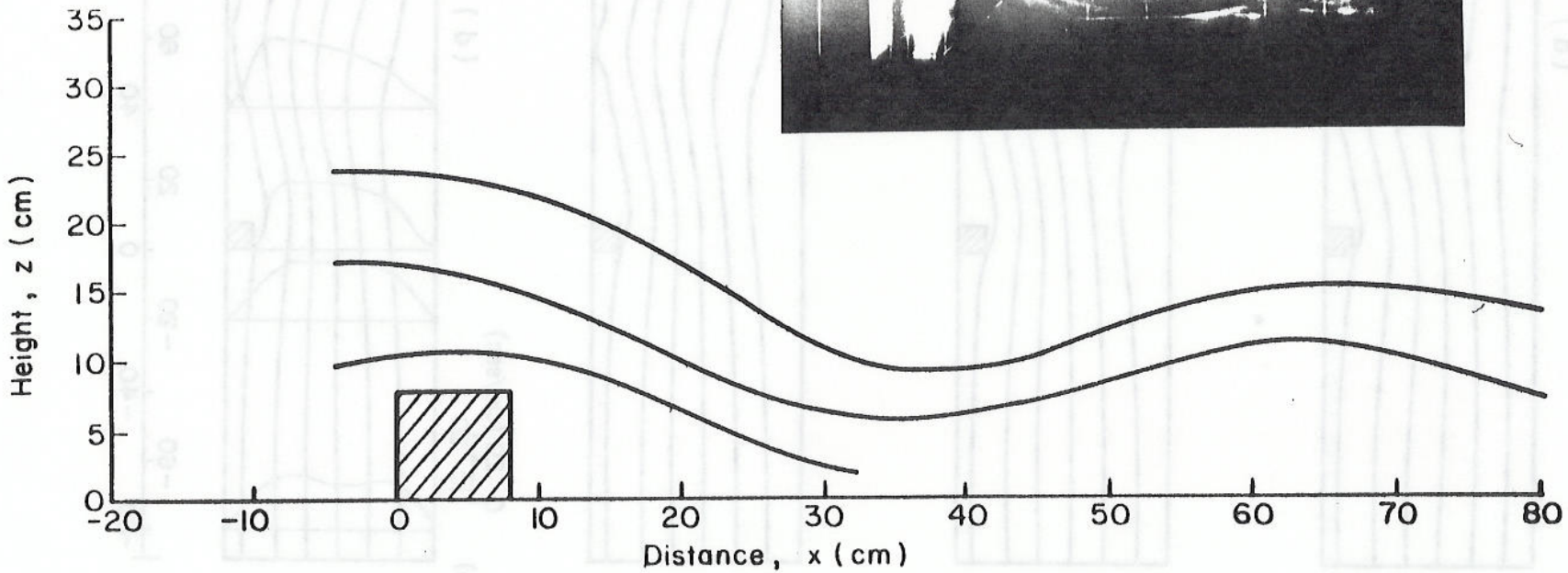
Height , z (cm)
35
30
25
20
15
10
5
0
-20
-10
0
10
20
30
40
50
60
70
80
Distance , x (cm)

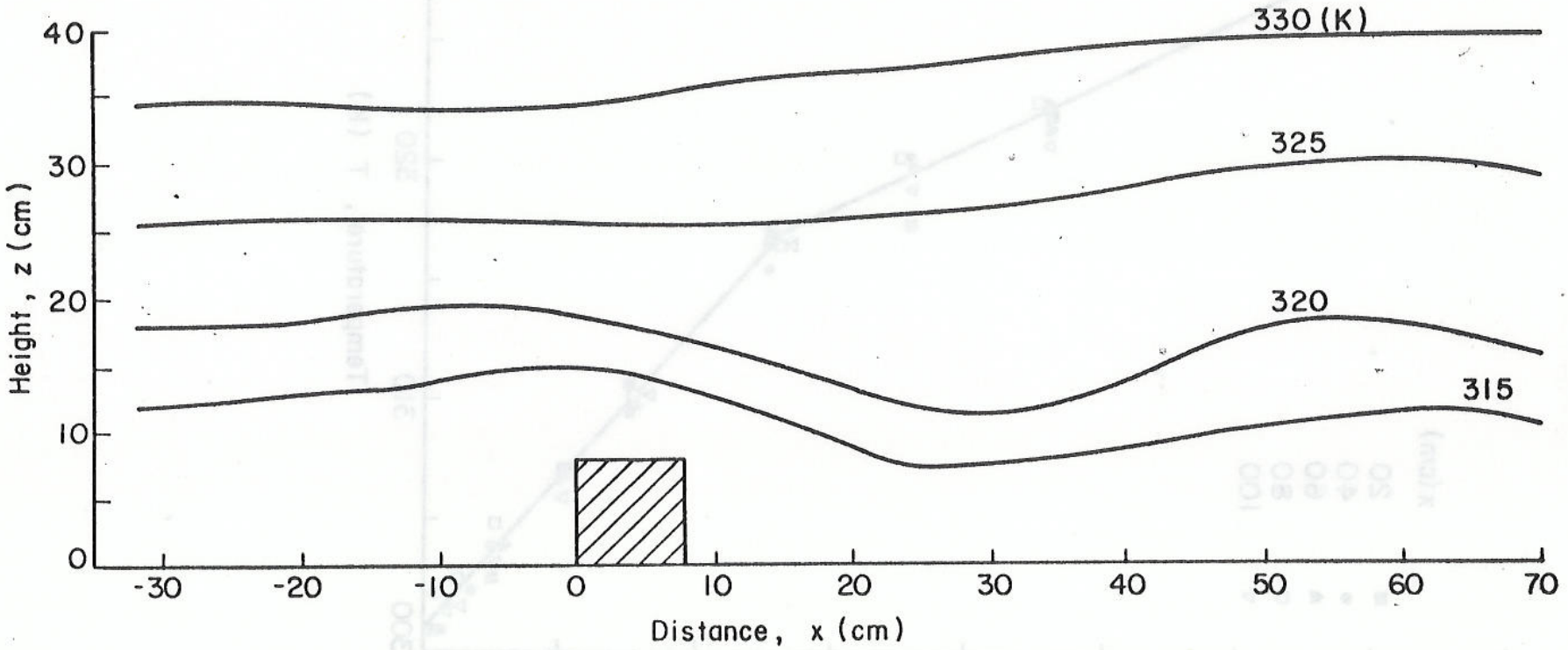
330 (K)
325
320
315
40
30
20
10
0
Height, z (cm)
-30
-20
-10
0
10
20
30
40
50
60
70
Distance, x (cm)

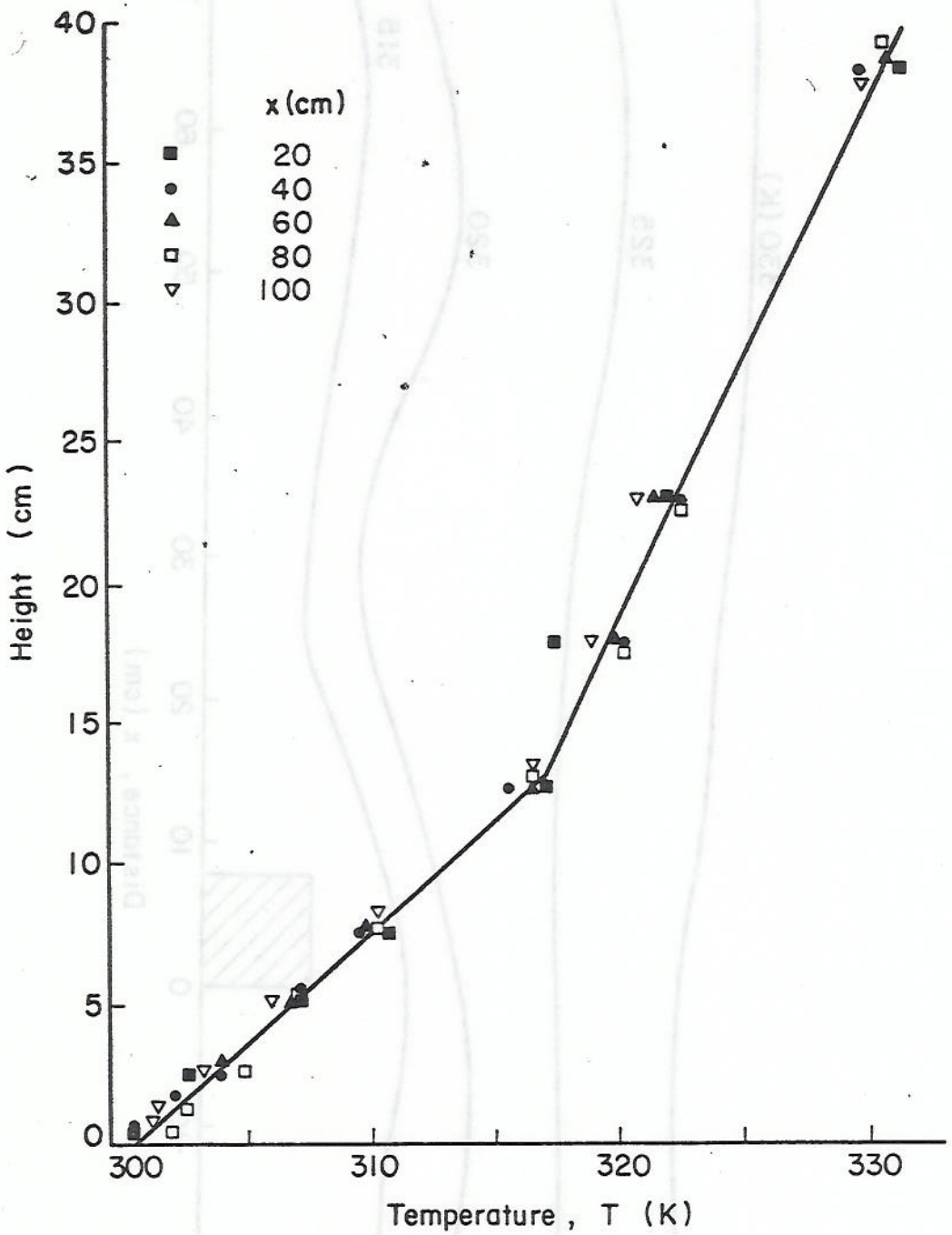
x (cm)
20
40
60
80
100
Height (cm)
0
5
10
15
20
25
30
35
40
300
310
320
330
Temperature , T (K)

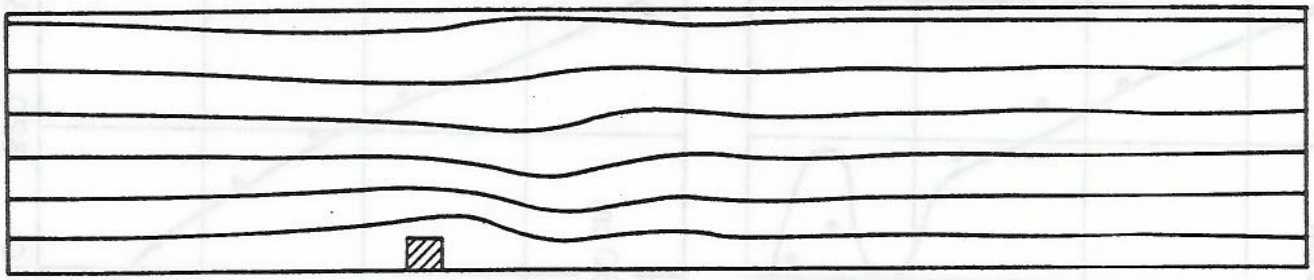

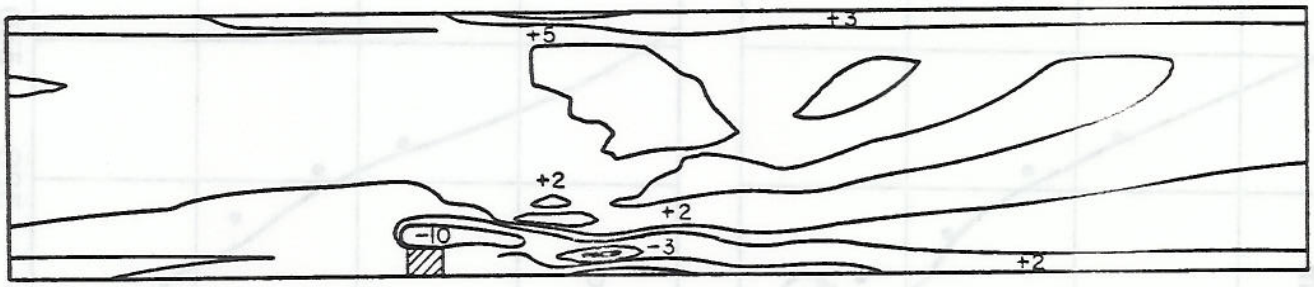
+5
+3
+2
+2
-10
-3
+2

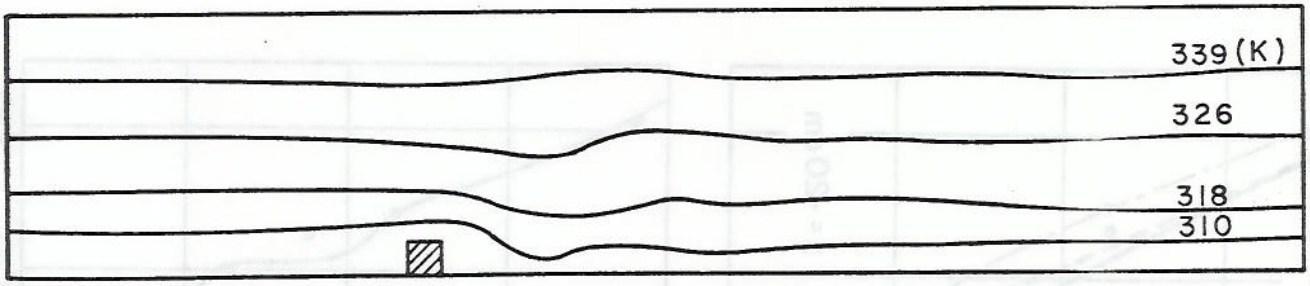
339 (K)
326
318
310

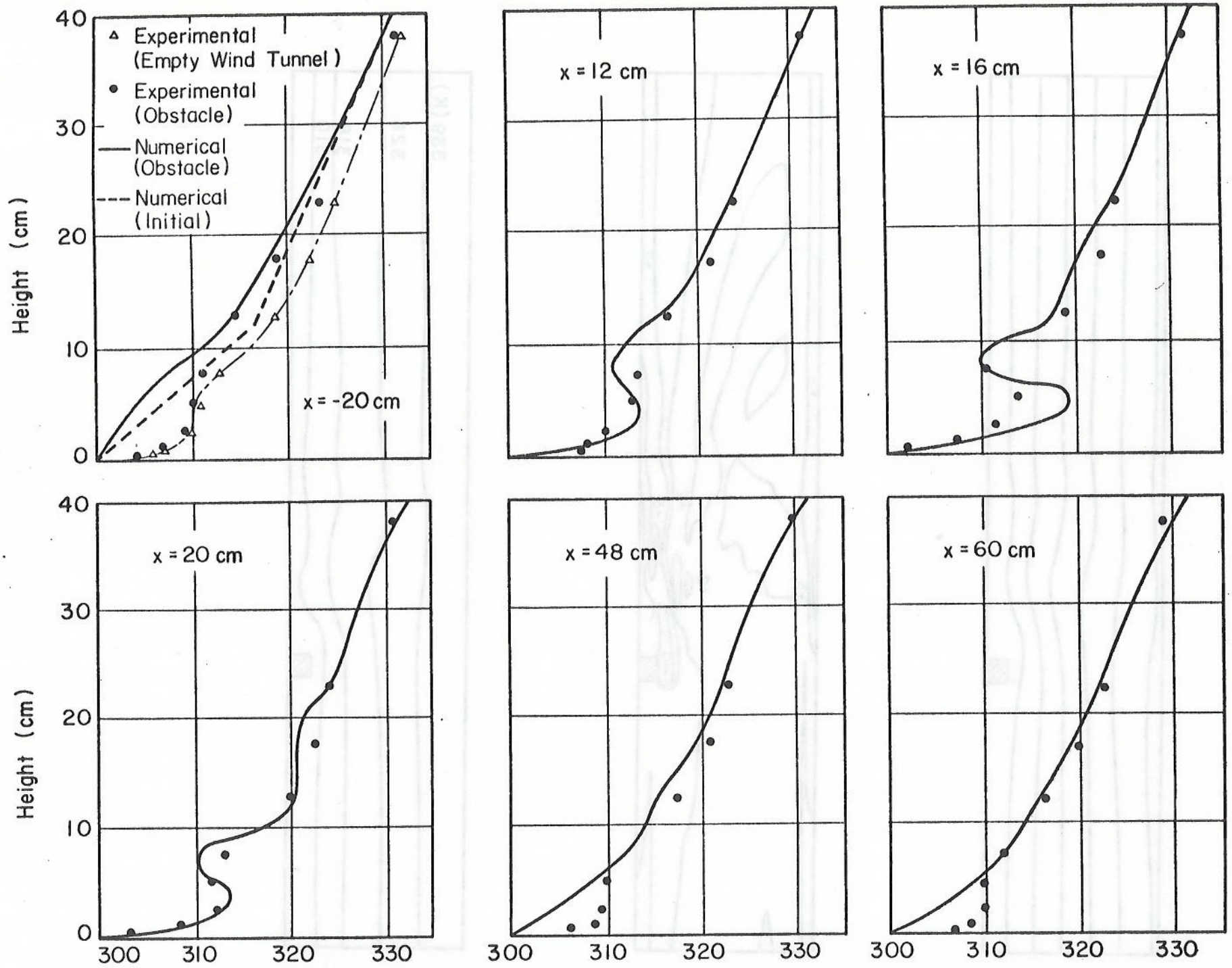
Experimental (Empty Wind Tunnel)
Experimental (Obstacle)
Numerical (Obstacle)
Numerical (Initial)
x = -20 cm
x = 12 cm
x = 16 cm
x = 20 cm
x = 48 cm
x = 60 cm
Height (cm)
Height (cm)
0
10
20
30
40
300
310
320
330

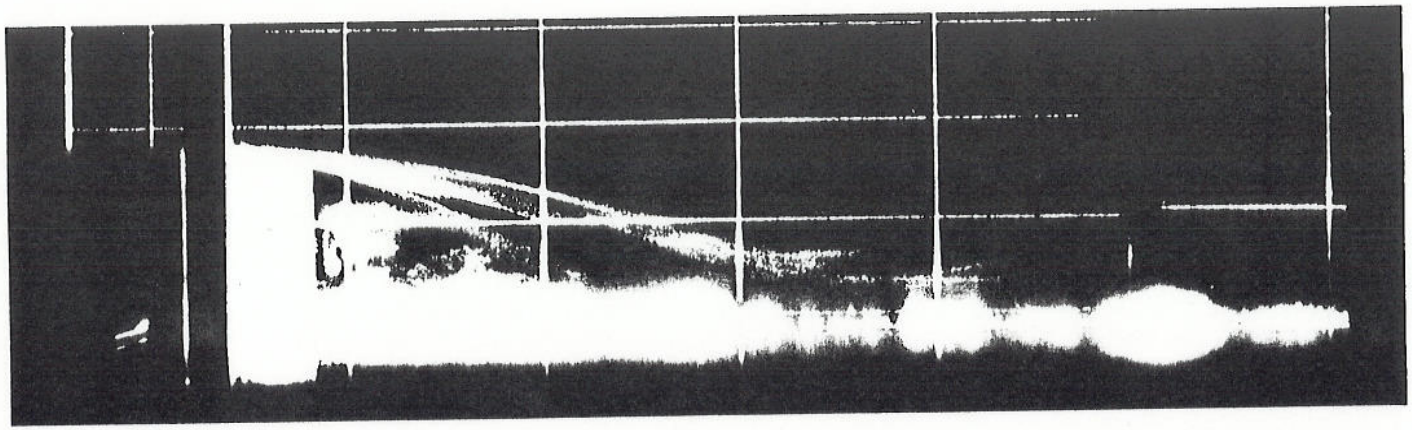

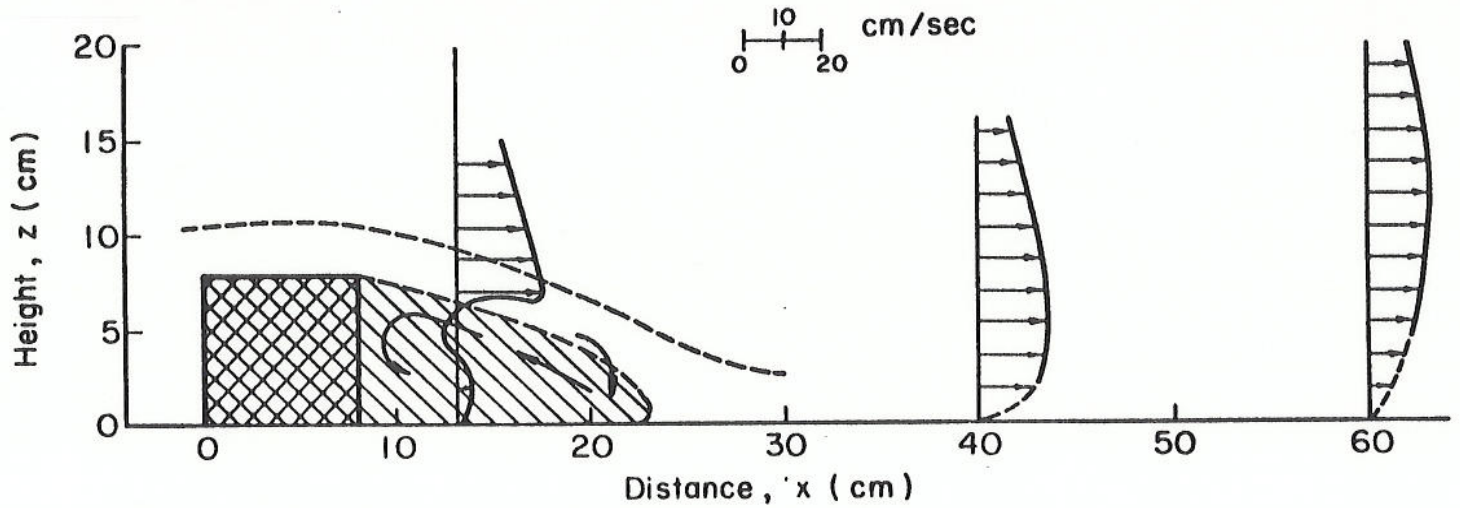
10
cm/sec
0
20
20
15
10
5
0
Height, z (cm)
0
10
20
30
40
50
60
Distance, x (cm)